



## OPEN ACCESS

## EDITED BY

Azeez Abdullah Barzinjy,  
Soran University, Iraq

## REVIEWED BY

Geetanjali Shukla,  
Captura Corp, United States  
Basem E. Keshta,  
Tanta University, Egypt

## \*CORRESPONDENCE

Oumayma Sbei,

✉ [oumayma.sbei@isbm.u-monastir.tn](mailto:oumayma.sbei@isbm.u-monastir.tn)

Anis Elaoud,

✉ [anis.aoud@yahoo.fr](mailto:anis.aoud@yahoo.fr)

<sup>†</sup>These authors have contributed equally to this work and share first authorship

RECEIVED 13 October 2025

REVISED 01 December 2025

ACCEPTED 15 January 2026

PUBLISHED 18 February 2026

## CITATION

Sbei O, Elaoud A, Ben Salah E, Tlili H, Mechi A, Salghi R, Ferhi M and Alabduly AJ (2026) Fe<sub>3</sub>O<sub>4</sub> nanoparticles synthesized via green *Eucalyptus globulus* extract for fluoride removal under magnetic treatment.

*Front. Environ. Sci.* 14:1723208.

doi: 10.3389/fenvs.2026.1723208

## COPYRIGHT

© 2026 Sbei, Elaoud, Ben Salah, Tlili, Mechi, Salghi, Ferhi and Alabduly. This is an open-access article distributed under the terms of the [Creative Commons Attribution License \(CC BY\)](https://creativecommons.org/licenses/by/4.0/). The use, distribution or reproduction in other forums is permitted, provided the original author(s) and the copyright owner(s) are credited and that the original publication in this journal is cited, in accordance with accepted academic practice. No use, distribution or reproduction is permitted which does not comply with these terms.

# Fe<sub>3</sub>O<sub>4</sub> nanoparticles synthesized via green *Eucalyptus globulus* extract for fluoride removal under magnetic treatment

Oumayma Sbei<sup>1,2\*†</sup>, Anis Elaoud<sup>2\*†</sup>, Eman Ben Salah<sup>3</sup>, Hajer Tlili<sup>4</sup>, Amani Mechi<sup>4,5</sup>, Rachid Salghi<sup>6</sup>, Mounir Ferhi<sup>4</sup> and Abdullah J. Alabduly<sup>7</sup>

<sup>1</sup>Higher Institute of Biotechnology of Monastir, University of Monastir, Monastir, Tunisia, <sup>2</sup>Research Laboratory of Environmental Sciences and Technologies, Higher Institute of Environmental Sciences and Technology, University of Carthage, Borj Cedria, Tunisia, <sup>3</sup>Faculty of Business Studies, Arab Open University, Riyadh, Saudi Arabia, <sup>4</sup>Laboratory of Physico-Chemistry of Mineral Materials and Their Applications, National Center for Research in Materials Sciences, University of Carthage, Borj Cedria, Tunisia, <sup>5</sup>Faculty of Science of Bizerte, University of Carthage, Bizerte, Tunisia, <sup>6</sup>Euro-Mediterranean University of Fes, Fez, Morocco, <sup>7</sup>Carbon Management Technology Institute, King Abdulaziz City for Science and Technology, Riyadh, Saudi Arabia

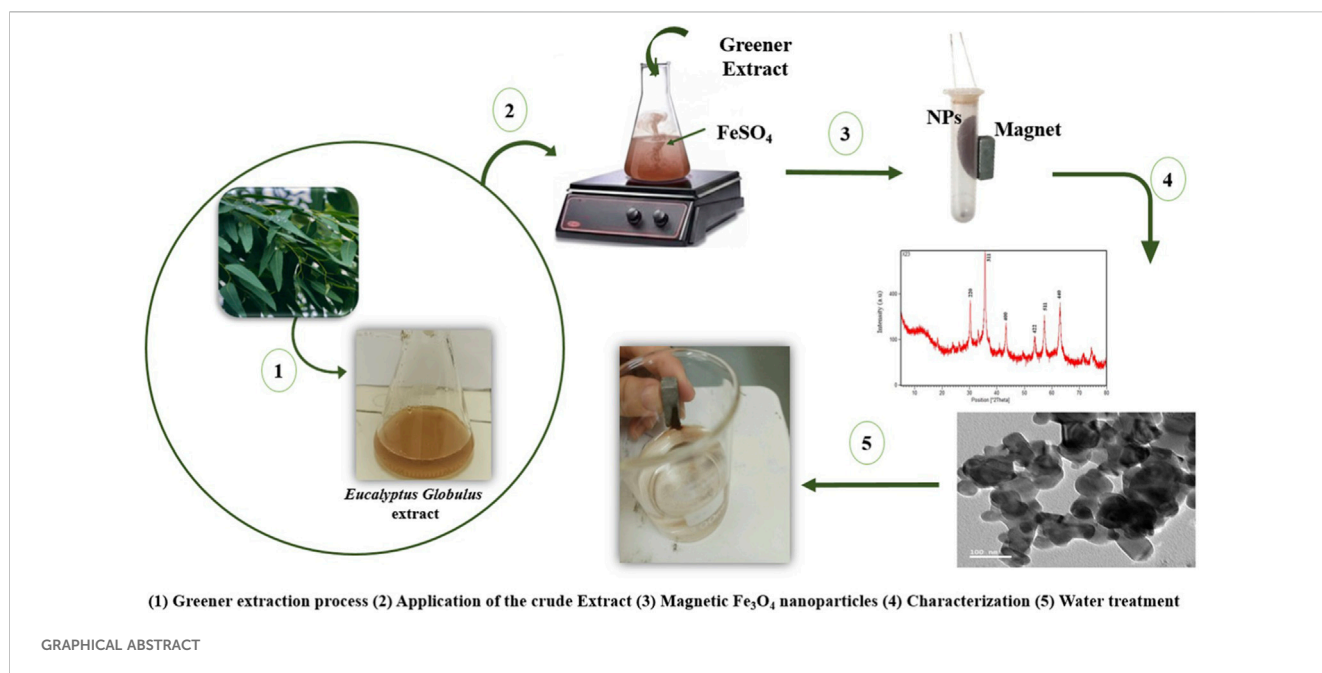
**Introduction:** Magnetite (Fe<sub>3</sub>O<sub>4</sub>) nanoparticles present physical and chemical properties with a great potential opportunity for biotechnology applications. This paper is about the green synthesis of Fe<sub>3</sub>O<sub>4</sub> nanoparticles from *Eucalyptus globulus* extract, which proves to be an adequate reductant in green chemistry because active polyphenols are abundantly available in it.

**Methods:** Using an extract of *E. globulus*, Fe<sub>3</sub>O<sub>4</sub> nanoparticles were created using the green coprecipitation method. X-ray Diffraction (XRD), Scanning Electron Microscopy (SEM), Energy Dispersive Spectroscopy (EDS), and Vibrating Sample Magnetometry (VSM) were used to analyze the colloidal particles that were produced. To determine the variables that affect the removal of fluoride from water, batch tests have been conducted. Contact time, adsorbent dosage, stirring speed, starting fluoride concentration, temperature, particle size, regeneration, and magnetization are the variables under investigation.

**Results and discussion:** Colloidal particles were obtained with super good magnetic property and easy dispersion in water. The results of XRD, EDS analyses have shown that pattern results of Fe<sub>3</sub>O<sub>4</sub> magnetic nanoparticles are consistent. The size distribution of iron nanoparticles from SEM images has revealed different sizes between 30 and 60 nm and also confirmed that the iron nanoparticles are ferrimagnetic. VSM analysis has proved that the saturation magnetization (Ms) value which was measured is 15.797 emu/g. These nanoparticles effectively eliminated fluoride ions, and with just a slight decrease in their adsorption capability, they can be regenerated and used for additional treatments. Additionally, the employment of a magnetic device and nanoparticles increased the fluoride ion adsorption effectiveness from 38% to 44%. These findings demonstrate the good magnetic strength and appropriate adsorption capacity of green produced Fe<sub>3</sub>O<sub>4</sub> nanoparticles from *E. globulus* extract, making them a promising environmentally friendly material for water treatment applications.

## KEYWORDS

adsorption, fluoride removal, iron oxide, nanoparticles, treatment



## 1 Introduction

Water scarcity and quality represent critical environmental challenges globally. Among these, the contamination of water with fluoride stands out as particularly concerning (Ravulapalli and Kunta, 2017; Dhillon et al., 2017). This issue arises from both natural occurrences and human activities. Notably, the World Health Organization has identified specific contaminants: arsenic, nitrate, and fluoride ions as particularly harmful to groundwater, highlighting the severity of this problem (Ravulapalli and Kunta, 2017).

Fluoride ions naturally occur in water, soil, plants, and animals, and at low concentrations, they are not harmful. However, exceeding the recommended limit of 1.5 mg/L in drinking water can cause adverse effects such as dental and skeletal fluorosis (Yadav et al., 2018; Cronin et al., 2000). Therefore, controlling fluoride levels is essential to protect public health. Fluoride ions are chemically stable and persistent in the environment, meaning they accumulate unless actively removed (Dhillon et al., 2017; Amini et al., 2008). Fluoride contamination originates from both natural and anthropogenic sources (Amini et al., 2008; Ali et al., 2016). Natural sources include geological processes such as mineral weathering, volcanic activity, hydrothermal vents, and marine aerosols, which can elevate fluoride levels in groundwater. Anthropogenic sources are often localized but significant, arising from industrial effluents, including coal-fired power plants, material processing facilities, and the use of products such as disinfectants, pesticides, and plastics (Ravulapalli and Kunta, 2017; Ali et al., 2016; Cronin et al., 2000).

Agricultural practices, particularly the uncontrolled use of phosphate fertilizers over an extended period, can also contribute to this issue (Ali et al., 2016). Indeed, the application of fluoride-rich water increases its content in soils (Yadav et al., 2018). In addition, exposed plants to high concentrations of fluoride show reduced root

growth, decreased biomass production, and loss of yield observed in different species (Cronin et al., 2000; Stevens et al., 2000). Bustingorri and Lavado (2014), proved that exceeding the concentration limit of fluoride (25 mg/L) has a negative impact on biomass and soybean yield. The shoots and roots are generally the most affected plant parts, showing chlorosis, necrosis, and structural damage (Yadav et al., 2018; Mackowiak et al., 2003). In another study, Mackowiak et al. (2003) demonstrated that a 30 mg/L fluoride concentration of irrigation water results in serious phyto-toxic trouble in rice, with a reduction of 60% in total biomass. The development of technologies for the elimination of excessive water fluoride becomes mandatory. Among the commonly used treatment techniques for the elimination of fluoride is the adsorption method (Srivastav et al., 2013).

Recently, nanotechnology has been developed, in particular the employment of nanoparticles (NPs), in various fields such as biology, environment, agriculture, electro-analysis, microfluidics, optical imaging, cosmetics, pharmaceuticals, medicine, biomedical fields, and specifically water treatment and purification (Iseli et al., 2009; Tran et al. 2010; Tlili et al., 2023a; Tlili et al., 2023b). Nanomaterials can be functionalized to acquire new properties and be adapted for specific applications by adjusting their size, shape, or crystal structure. Other surface characteristics like dispersion in different media, compatibility, and reactivity towards adsorption are also concerned. This functionalization is performed either by a change of the particles or by surface treatment using several strategies such as the coating of the nanoparticles with a surface layer to elaborate a core-shell structure, grafting of functional chemical groups and doping (Jolivet et al., 2010).

Nanomaterials are materials with an nm dimension varying until 100 nm. They are the bridge amongst atomic materials and bulk materials (Tran et al. 2010). Nanomaterials can take different shapes, including nanoparticles, nano-powders, nanofibers,

nanotubes, nanomembranes (Tran et al. 2010). Some nanomaterials exist in a natural state (dust, smoke, ...), while others are synthesized for specific applications (Tran et al. 2010). Nano-adsorbents used for water treatment are classified into three groups: carbon-based nano-adsorbents (activated carbon, carbon nanotubes, fullerenes, and graphene), metal nanoparticles like those that silver or iron and nano-adsorbents based on metal oxides (Kumari et al., 2019; Sbei et al., 2025; Abbas et al., 2025). The most important are nanoparticles based on zinc oxide, iron, titanium, and aluminum that are strong adsorbents of toxic heavy metals (Kumari et al., 2019; Sbei et al., 2025). Iron-based nanoparticles are recognized for their exceptionally great surface area in addition to rapid reactivity, which are important properties, making them environment-friendly and efficient water treatment agents (Mukhopadhyay et al., 2019). Alternatively, the metal oxides showed significant affinity to fluoride. More precisely, Bhatnagar et al. (2011) confirmed the affinity of iron oxides for fluoride ions. The iron oxide adsorption capacity for fluoride varies from 10 mg/g to 25 mg/g (Asuha et al., 2012; Iiu et al., 2016). Hematite ( $\alpha$ -Fe<sub>3</sub>O<sub>4</sub>), maghemite ( $\gamma$ -Fe<sub>2</sub>O<sub>3</sub>), and magnetite (Fe<sub>3</sub>O<sub>4</sub>) are the best-known iron oxides (Maiti and Devi, 2015). These iron oxide based nano-adsorbents have been mostly experimented by researchers to remove numerous pollutants from environmental or industrial effluents. The removed pollutant are Cr (VI), As (V), Cr<sub>2</sub>O<sub>7</sub><sup>2-</sup>, MnO<sub>4</sub><sup>-</sup>, Pb (II), Cu (II), and Hg (II) (Zargoosh et al., 2013). Magnetite, which is a natural mineral, can also be developed using solutions of ferric and ferrous ions. Iron nanoparticles are extremely pure and free from other harmful elements incorporating low levels of carbon, oxygen, nitrogen, phosphorus, and sulfur (Chiavola et al., 2016). Magnetite nanoparticles are widely employed as magnetic material to create magnetic adsorbents because of their relatively simple and easily controllable synthesis process, and their high magnetic characteristics compared to other iron oxides (Tolmacheva et al., 2016).

Iron oxide nanoparticles (Fe<sub>3</sub>O<sub>4</sub>) are promising materials used for water treatment because of numerous advantageous properties. In fact, they are stable, with a unique morphology and an important surface. In addition, they are easily separated through the employment of outer magnetic fields. These nanomaterials can serve as effective adsorbents, photo-catalysts, and coagulation agents for the purification of the water, depending on their superficial functionalities or composition (Martinez and Simeonidis, 2019; Sharma et al., 2018). Long-reactive iron nanoparticles with sizes ranging from 10 to 100 nm have been shown to be efficient in detoxifying pesticides, chlorine-containing compounds, polychlorinated biphenyls, and organic solvents (Zhang, 2003).

The use of nano-scale metals and metal oxide materials is gaining attention due to their excellent performance and cost-effectiveness in removing contaminants (Zhang et al., 2016). In the fluoride elimination from aqueous solutions, various inorganic nanomaterials including iron-based oxide of metal and composites, cerium, alumina, titanium, magnesia, zirconium, and calcium play a fundamental role in defluoridation processes (Hua et al., 2012).

Recent studies have contributed to a deeper understanding of magnetic iron oxide nanoparticles and their potential in sustainable water treatment technologies. These investigations emphasize advancements in green synthesis approaches, surface modification strategies, and adsorption performance optimization for wastewater

remediation (Keshta et al., 2024; Hussain et al., 2025; Javeria et al., 2025; Armaya'u et al., 2024). Collectively, these findings demonstrate that eco-friendly synthesis methods combined with magnetic coupling can enhance pollutant removal efficiency while minimizing environmental impact. This study has the objective of parameters optimization of Fe<sub>3</sub>O<sub>4</sub> nanoparticles with the perspective of treating fluoride in water, within the context of the emerging field of nanotechnology. By harnessing the distinctive physicochemical properties and the large ratio volume/surface, nanomaterials can be employed as effective separation supports for the purification of polluted water. The introduction of this novel technique for water treatment, which involves the use of nanoparticles, is imperative in order to address contemporary challenges and supplant conventional or expensive approaches.

## 2 Material and methodology

### 2.1 Method of nanoparticles Fe<sub>3</sub>O<sub>4</sub> synthesis

The green synthesis of iron nanoparticles using *Eucalyptus Globulus* extract involved a detailed and methodical process (Jolivet et al., 2002; Sbei et al., 2025). Initially, the leaves of *Eucalyptus Globulus* were meticulously collected, washed with distilled water, and air-dried at room temperature for 2 days. This step was crucial for ensuring the purity of the extract. Phytochemical screening was then conducted on the leaf extracts to identify various compounds such as tannins, saponins, alkaloids, phenols, and others, following the method outlined by Ugochukwu et al. (2013).

Dried *Eucalyptus* leaves (10 g) were boiled in 100 mL of Milli-Q water at 55 °C for 1 h under continuous stirring. The mixture was cooled for 1 h and filtered to obtain the aqueous extract. Subsequently, 1.5 g of FeSO<sub>4</sub> was dissolved in 30 mL of Milli-Q water, followed by the addition of 10 mL of the prepared *Eucalyptus* extract. The solution was then adjusted to a final volume of 200 mL with Milli-Q water in a 500 mL beaker. The pH was raised to 9–11 using 0.1 M NaOH to promote coprecipitation. The formation of Fe-NPs was indicated by a distinct black precipitation in the solution. The mixture was shaken for 24 h at ambient temperature, followed by centrifugation at 4,000 rpm for 15 min to separate the nanoparticles. The precipitate was washed three times with Milli-Q water, once with ethanol then centrifuged at 4,000 rpm for 15 min, frozen at -20 °C, and dried using an orbital shaker (IKA KS 3000 i control) at 155 rpm and 30 °C for 24 h to ensure uniform drying and prevent agglomeration. Finally, the dried nanoparticles were ground into a fine powder using a porcelain mortar. This controlled process guarantees reproducibility and preserves the magnetic properties associated with nanoparticle size and dispersion, in line with best practices for green synthesis reported in recent literature (Pandhare et al., 2025a; Al-Labadi et al., 2025) (Figures 1A,B).

### 2.2 Phytocomponent identification by GC-MS

*Eucalyptus globulus* leaf extracts compounds were elaborated and their relative percentages were measured by GC-MS analysis

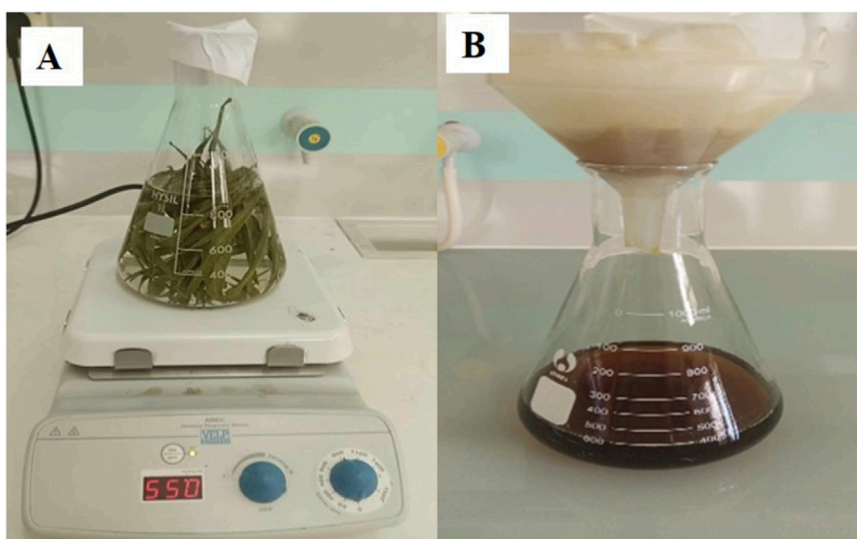


FIGURE 1 Extraction of *Eucalyptus globulus* process: (A) Missing distilled water and leaves under heating; (B) Filtered *E. Globulus* extract.

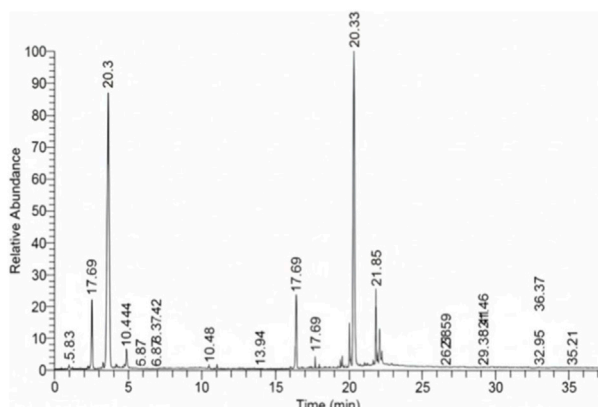


FIGURE 2 GC-MS chromatogram of ethanoic extract of *Eucalyptus globulus* (Sharma et al., 2024).

(Figure 2). The study emphasized 1,8-cineole (eucalyptol) as the major component, which is in perfect agreement with the previous results of other *Eucalyptus* species like *E. maidenii*, *E. nitens*, *E. dunnii*, and *E. grandis* (Barbosa et al., 2016; Dhakad et al., 2018). One of the main components of the majority of aromatic plants is eucalyptol or 1,8-cineole, which is highly recognized for its antioxidant, anti-inflammatory, antifungal, and antinociceptive effects (Miranda et al., 2016). Besides that, the GC-MS chromatogram tells us that the main compounds were eucalyptol (24.92%),  $\alpha$ -pinene (19.34%), and  $\alpha$ -guaiene (15.17%), while  $\alpha$ -terpineol (9.49%) and (-)-spatulanol (10.60%) were significantly present as well. Furthermore, the leaf terpenoid profile of *E. globulus* was enriched with a few minor volatile compounds, namely,  $\gamma$ -himachalene,  $\delta$ -selinene,  $\alpha$ -copaene, and nootkatone-11, 12-epoxide (Sharma et al., 2024).

## 2.3 Characterization of $\text{Fe}_3\text{O}_4$ nanomaterials

The structural characteristics of  $\text{Fe}_3\text{O}_4$  nanoparticles were analyzed both before and after the adsorption of fluoride ions. This analysis was carried out using a Quanta FEG 650 model Scanning Electron Microscope (SEM) at a setting of 10 kV, with a magnification of 120,000 and a working distance of 12.1 mm. Additionally, to examine the chemical composition, an Energy Dispersive X-ray (EDS) detector was employed on the same SEM model, operating at 10 kV. Further, the crystal structure of the synthesized product was explored using a Bruker D8 Advance high-resolution X-ray powder diffractometer (XRD), utilizing Cu-K $\alpha$  radiation (1.5418 Å). Average particle size is determined by measuring widths at half-height and using the following Debye Scherrer relationship (Simon-Deckers et al., 2009):

$$D = \frac{k\lambda}{\beta \cos \Theta}$$

With D is the particle size in nm, K is the Scherrer constant (approximately 0.9 for spherical particles),  $\lambda$  is the wavelength of the radiation used ( $\lambda = 1.54056 \text{ \AA}$ );  $\beta$  is the width a mis height in radian and  $\Theta$  is the position of the diffraction peak considered (in  $\theta$ ).

Using a Lakeshore 7404 Series vibrating sample magnetometer (VSM), magnetic properties were examined. Magnetization (M) versus applied magnetic field (H) was measured in the range of  $-20$  to  $+20,000$  Oersted at  $150 \text{ }^\circ\text{C}$ . This information revealed the magnetic behavior and suitability of the nanoparticles for magnetic separation applications.

## 2.4 Treatments of fluorinated solutions by nanoparticles

A Total Ionic Strength Adjustment Buffer (TISAB) solution plays a crucial role in accurately determining fluoride concentration.

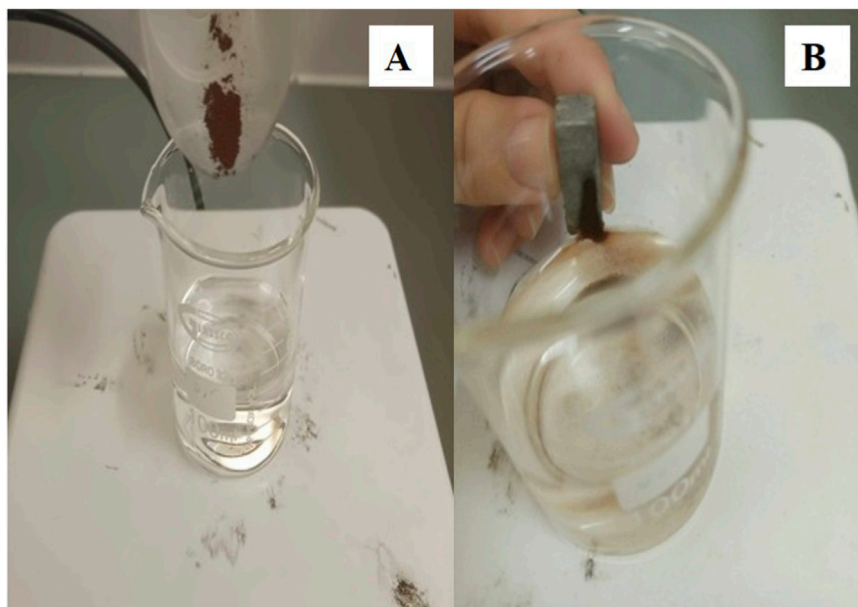


**FIGURE 3**  
(A) Nanoparticles purify water for a predetermined time while stirring; (B) Post-treatment recovery of nanoparticles.

It not only adjusts the pH but also disintegrates complex fluoride compounds, allowing for an accurate measurement of fluoride ions. The preparation of TISAB involves combining 58 g of sodium chloride and 57 mL of glacial acetic acid in 500 mL of distilled water. Subsequently, the solution's pH is adjusted to 5 using 5M sodium hydroxide, typically by adding around 15 pellets, with continuous stirring for even distribution. Fluoride ions were tested in the following elimination experiments: A fluoride solution with a 25 mg/L concentration was prepared from a stock sodium fluoride solution (NaF, 100 mg/L). The  $\text{Fe}_3\text{O}_4$  nanoparticles were supplemented to a 0.03 L solution with a dose of 0.02 g to several samples of the prepared solution and each sample was stirred at 200 rpm for a predefined time for each sample while maintaining the temperature at 30 °C with a pH of 7. After each treatment, the nanoparticles were assembled using a hand-held permanent magnet, while the supernatant was exploited to measure the remaining fluoride ions (Figure 3).

The fluoride concentration was determined using a fluoride ion-selective electrode. Specifically, 15 mL of each treated sample was mixed with 1.5 mL of the TISAB solution, and the fluoride ion concentration was measured using a calibrated ion-selective electrode connected to a potentiometer or ion meter.

#### 2.4.1 Contact time

Every experiment was repeated three times accordingly; For 1 hour, measurements of the residual fluoride ion concentration,  $C_t$ , are made every 10 min.  $\text{Fe}_3\text{O}_4$  nanoparticles are used to methodically set the starting concentration,  $C_0$ , at 25 mg/L. Calculating the adsorption capacity and removal efficiency requires knowing the values of the residual concentrations,  $C_t$ . average values were recorded for the calculation of removal efficiency (E) and adsorption capacity (A) were computed as follows:

$$A(\text{mg/L}) = \frac{(C_0 - C_t) \times V}{M} \quad E(\%) = \frac{C_0 - C_t}{C_0} \times 100$$

Where A is the adsorption capacity in mg/g,  $C_0$  is the initial fluoride ion concentration in mg/L,  $C_t$  is the remaining fluoride ion concentration after incubation for t minutes in mg/L, V is the solution volume in liters, M is the mass of  $\text{Fe}_3\text{O}_4$  nanoparticles in grams and E is the removal efficiency in percentage.

#### 2.4.2 Mass of nanoparticles

In order to choose the optimal adsorbent quantity (magnetite nanoparticles) needed to obtain quantitative recoveries of fluoride ions, different amounts of adsorbent ranging between 0.01 and 0.1 g were used in treatment trials for 45 min with a 30 °C temperature, a pH of 7, a 200 rpm stirring speed, and a 25 mg/L initial concentration of fluoride ions.

#### 2.4.3 Stirring speed

The effect of stirring speed on fluoride adsorption was investigated by varying the stirring rate from 0 to 600 rpm. The experiments were conducted using 0.02 g of iron oxide nanoparticles for 45 min at pH 7 °C and 30 °C, with an initial fluoride ion concentration of 25 mg/L.

#### 2.4.4 Regeneration

After the previous treatments, the nanoparticles were collected by an external magnetic field (Kumari et al., 2019). After that, they were recovered and dried for 3 h and they are used for the fluoride treatment for 45 min, at a stirring speed of 200 rpm, a temperature of 30 °C, and a pH of seven. The recovered nanoparticles were then reused for additional treatments. Each treatment was repeated three times and the average values are reported to determine the regeneration effect on the adsorption capacity of the nanoparticles.

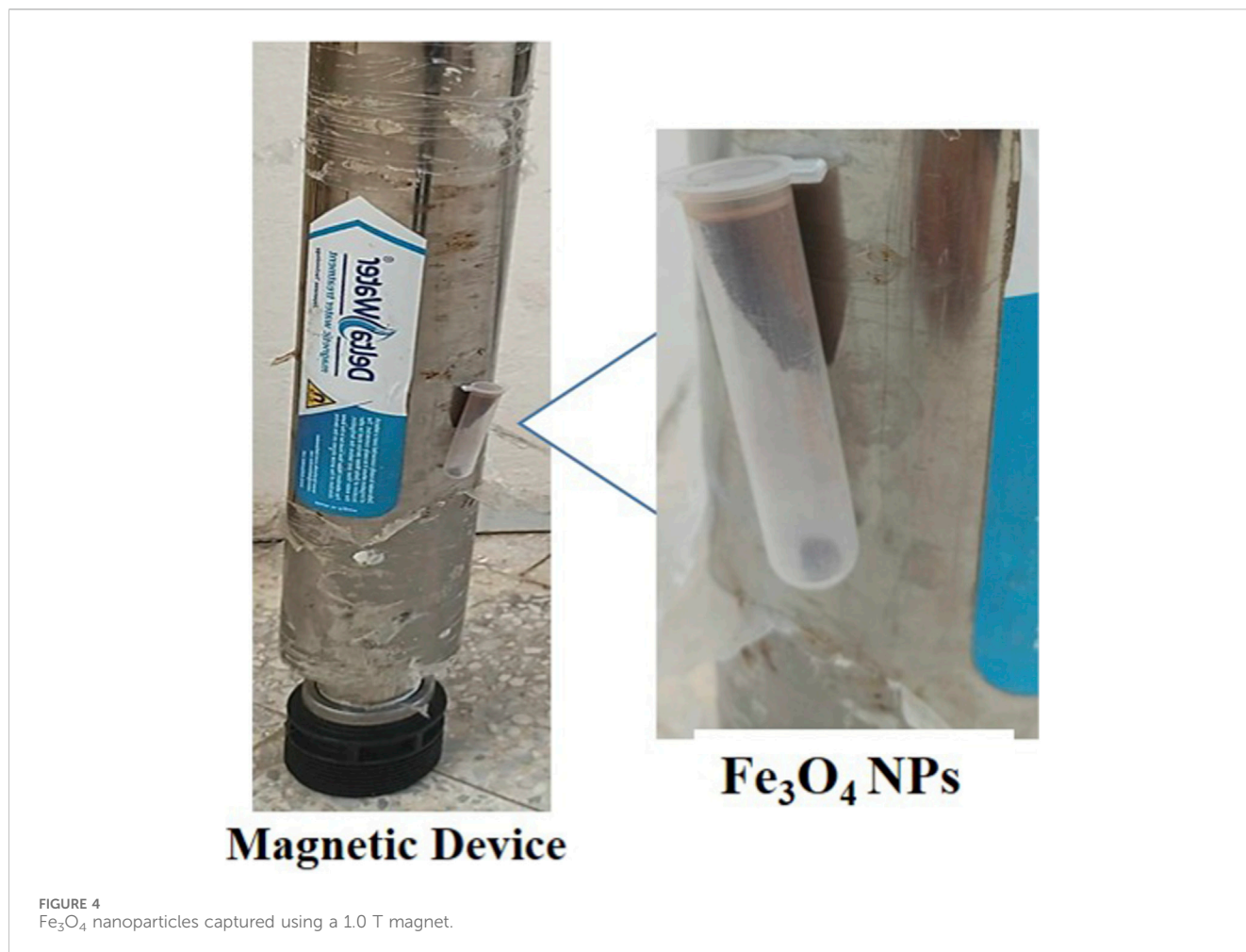


FIGURE 4  
 $\text{Fe}_3\text{O}_4$  nanoparticles captured using a 1.0 T magnet.

The adsorbent concentration can significantly influence the pollutants removal from aqueous solutions. Subsequently, the effect of the initial fluoride ion concentration was studied by preparing several solutions with concentrations varying from 20 mg/L to 100 mg/L. These solutions were treated with  $\text{Fe}_3\text{O}_4$  nanoparticles for 45 min with stirring at 200 rpm at a neutral pH and a 30 °C temperature. Average values were plotted to calculate both the removal efficiency and adsorption capacity.

#### 2.4.5 Temperature

The temperature variation from 20 °C to 80 °C was applied by setting the other parameters as follows: nanoparticles dose of 0.02 g, a 25 mg/L initial fluoride concentration, a neutral pH, a 45 min contact time, and a stirring of 200 rpm.

#### 2.4.6 Nanoparticles-magnetization coupling

The impact of two different treatment techniques on the concentration of fluoride ions was evaluated. In the first treatment, only  $\text{Fe}_3\text{O}_4$  nanoparticles were used, whereas the second treatment combined  $\text{Fe}_3\text{O}_4$  nanoparticles with a magnetic device. For both treatments, the initial fluoride concentration ( $C_0$ ) was maintained at 25 mg/L, with a contact time of 45 min, at 30 °C, and neutral pH. During the second treatment, the water was exposed to a permanent magnetic field of 1 T using an installed magnetic

device, enabling simultaneous nanoparticle adsorption and magnetic treatment.

## 3 Results and discussion

The synthesized  $\text{Fe}_3\text{O}_4$  nanomaterials appear as a black powder. Notably,  $\text{Fe}_3\text{O}_4$  is water-soluble, forming a black colloidal solution when mixed with water. The magnetic properties of these nanomaterials are demonstrated in Figure 4, where their behavior under the influence of a magnet is shown. This evidence confirms the strong magnetic characteristics of the  $\text{Fe}_3\text{O}_4$  nanomaterials.

### 3.1 Nanoparticles characterization

#### 3.1.1 Scanning electron microscopy (SEM) analysis

SEM imaging was carried out using an FEI Quattro S microscope operating at an accelerating voltage of 15 kV. The powdered  $\text{Fe}_3\text{O}_4$  sample was mounted on a flat holder and sputter-coated with a 10 nm copper layer to minimize charging effects. Micrographs were obtained to examine the morphology and size distribution of the synthesized magnetite nanoparticles (Sbei et al., 2025; Elaoud et al., 2024). Figure 5A shows  $\text{Fe}_3\text{O}_4$

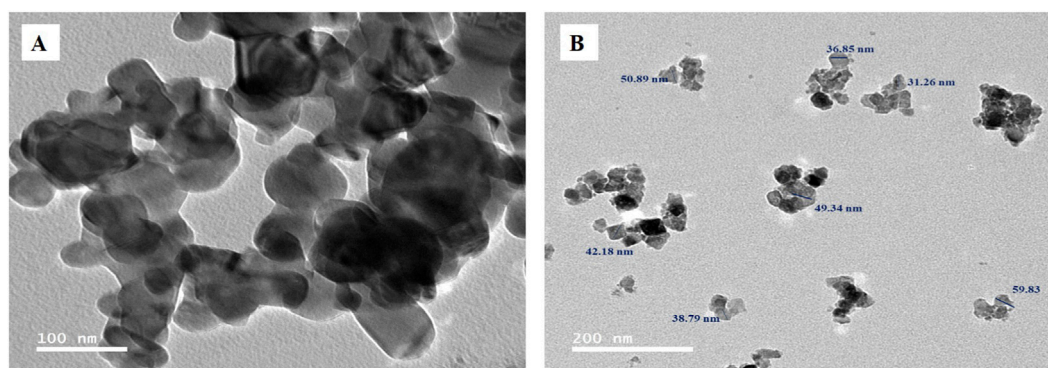


FIGURE 5 (A) SEM image of produced  $\text{Fe}_3\text{O}_4$  nanomaterials; (B) SEM image of regenerated  $\text{Fe}_3\text{O}_4$  nanoparticles.

nanoparticles before fluoride adsorption. The particles tend to form dense nano-scale aggregates and exhibit near-spherical to angular/granular shapes, which aligns with previous reports on green-synthesized magnetite nanoparticles (Elaoud et al., 2024; Pandhare et al., 2025a). Measurements taken directly from the micrograph indicate particle sizes ranging from 31.26 to 59.83 nm, with an average size of 44.16 nm and a sample standard deviation of 9.75 nm.

These values fall within the expected range of 30–60 nm, typical for  $\text{Fe}_3\text{O}_4$  nanoparticles exhibiting ferrimagnetic properties (Sbei et al., 2025). Similar aggregation behavior has been observed in  $\text{TiO}_2/\text{Fe}_3\text{O}_4$  based nanomaterials during phase transitions (O'Byrne et al., 2024), highlighting the influence of surface energy and magnetic interactions on cluster formation.

In contrast, Figure 5B presents the regenerated  $\text{Fe}_3\text{O}_4$  nanoparticles after fluoride adsorption and desorption. The morphology changes significantly: micro-scale agglomerates have formed, and the particles appear more irregular and fused compared to their initial state. The boundaries between particles are less distinct, and the clusters display a compact, dense structure, suggesting strong antiparticle adhesion or partial sintering. These changes point to surface restructuring, likely caused by fluoride interaction with surface hydroxyl groups, which alters surface charge and reduces electrostatic repulsion. Combined with magnetic dipole-dipole forces, this promotes irreversible aggregation during regeneration. Such morphological evolution can substantially reduce the number of accessible active sites, ultimately affecting adsorption efficiency in subsequent cycles (Pandhare et al., 2025a; Sbei et al., 2025).

### 3.1.2 X-ray diffraction (DRX)

The XRD pattern of the synthesized  $\text{Fe}_3\text{O}_4$  nanoparticles (Figure 6) exhibits six distinct diffraction peaks at  $2\theta$  values of  $30.3^\circ$ ,  $35.6^\circ$ ,  $43.1^\circ$ ,  $53.7^\circ$ ,  $57^\circ$ , and  $62.7^\circ$ , corresponding to the (220), (311), (400), (422), (511), and (440) planes, respectively (Ganapathe et al., 2020). These peaks match the standard JCPDS card 01-073-2273, confirming the formation of magnetite with a cubic spinel structure and the absence of secondary phases. This observation is consistent with previous studies on  $\text{Fe}_3\text{O}_4$  nanoparticles (Gemeay et al., 2020; Keshta and Gemeay, 2022; El-Shater et al., 2024). To

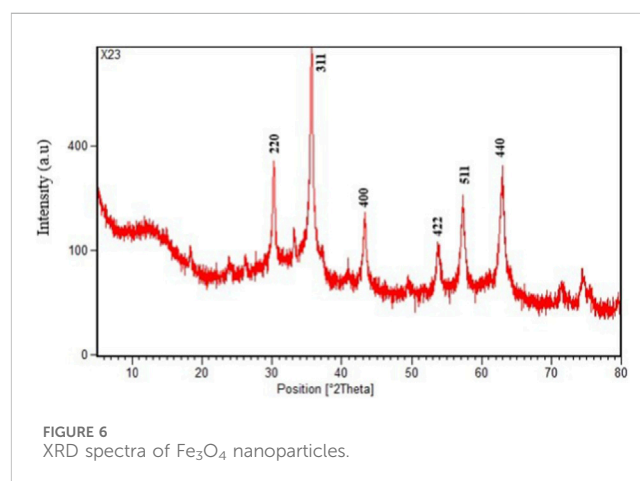


FIGURE 6 XRD spectra of  $\text{Fe}_3\text{O}_4$  nanoparticles.

further characterize the crystallinity, the average crystallite size was calculated using the Scherrer equation applied to the (311) reflection ( $2\theta \approx 35.6^\circ$ ), with  $K = 0.9$  and  $\text{Cu-K}\alpha$  radiation ( $\lambda = 0.154056$  nm). Assuming an average FWHM of  $0.4^\circ$  ( $2\theta$ ), the estimated crystallite size was approximately 21 nm. This value is smaller than the SEM-observed particle size (30–60 nm), which is expected because SEM measures aggregated particles, while XRD determines the size of individual crystallites. Similar discrepancies between crystallite and particle sizes have been reported for  $\text{Fe}_3\text{O}_4$  nanoparticles synthesized via green and polyol methods (Pandhare et al., 2025a; Pandhare et al., 2025b).

### 3.1.3 Energy Dispersive X-ray spectrometer (EDS)

Figure 6 shows the Energy Dispersive X-ray Spectroscopy (EDS) spectrum of the synthesized  $\text{Fe}_3\text{O}_4$  nanoparticles and the regenerated  $\text{Fe}_3\text{O}_4$  nanoparticles after reuse. The main peaks correspond to iron (Fe) and oxygen (O), confirming the expected elemental composition of magnetite. The absence of any additional elements indicates the high purity of the prepared material and the effectiveness of the washing process (Figure 7A) (Elaoud et al., 2024; Sbei et al., 2025).

For the regenerated sample, the EDS pattern shows the same Fe and O signals, demonstrating that the nanoparticles retained their

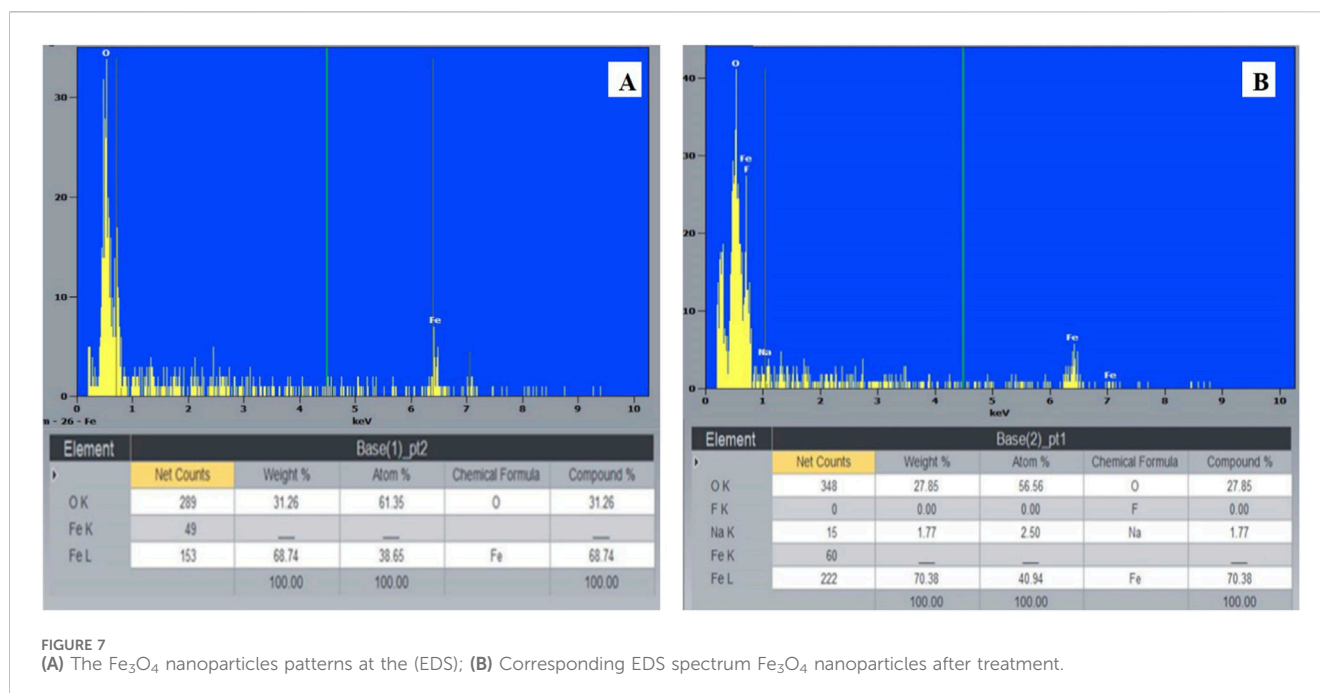


FIGURE 7 (A) The  $\text{Fe}_3\text{O}_4$  nanoparticles patterns at the (EDS); (B) Corresponding EDS spectrum  $\text{Fe}_3\text{O}_4$  nanoparticles after treatment.

structural composition after repeated use. The calculated O/Fe atomic ratio, close to the stoichiometric value expected for  $\text{Fe}_3\text{O}_4$ , further supports the successful formation and stability of the magnetite phase (Figure 7B) (Thili et al., 2023a; Thili et al., 2023b).

$$\text{O/Fe atomic ratio} = \frac{\text{Atom \% O}}{\text{Atom \% Fe}}$$

$$\text{O/Fe atomic ratio} = \frac{56.56}{40.94} = 1.38$$

### 3.1.4 Vibrating sample magnetometer (VSM)

The magnetic characteristics of  $\text{Fe}_3\text{O}_4$  nanoparticles were evaluated using a vibrating sample magnetometer (VSM) (Lakeshore 7404 Series), providing valuable insights into their magnetic behavior (Ismail et al., 2023). The magnetization curve (Figure 8) and magnetic parameters (Table 1) confirm the ferrimagnetic nature of the synthesized nanoparticles at ambient temperature. The measured remnant magnetization was 2.7242 emu/g, and the coercivity was 196.89 Oe, indicating low magnetic hysteresis and suitability for magnetic separation applications (Goya et al., 2003; Mahmed et al., 2011). The saturation magnetization ( $M_s$ ) reached 15.797 emu/g, which is lower than bulk  $\text{Fe}_3\text{O}_4$  ( $\approx 92$  emu/g) due to surface spin disorder and organic capping from the green synthesis process. However, this value is comparable to recent reports for green-synthesized  $\text{Fe}_3\text{O}_4$  nanoparticles (14–18 emu/g), confirming that eco-friendly synthesis does not compromise magnetic performance (Keshta et al., 2024; Al-Labadi et al., 2025; Sbei et al., 2025). These results demonstrate that the prepared nanoparticles exhibit sufficient magnetic strength for efficient recovery and reuse in water treatment applications.

## 3.2 Study of fluoride adsorption with several factors

### 3.2.1 Variation of the contact time

The duration of contact between the adsorbent and the fluoride ions plays an important role in determining adsorption efficiency. As shown in Figure 9, fluoride adsorption increased rapidly during the first 45 min, with the adsorption capacity rising from 7.35 to 14.5  $\text{mg g}^{-1}$ . This fast initial uptake is mainly due to the large number of available active sites and the strong driving force for fluoride transfer to the nanoparticle surface. After 45 min, the adsorption capacity reached equilibrium and showed little further change, indicating that most active sites were already occupied and some pores may have become blocked.

The equilibrium time of 45 min can therefore be considered optimal under the present experimental conditions. Although similar behaviors have been observed in other studies (Hafshejani et al., 2017), the exact equilibrium time often varies depending on factors such as material properties, particle size, and operating conditions.

### 3.2.2 Adsorption kinetics

The adsorption data were fitted to pseudo-first-order and pseudo-second-order kinetic models to identify the rate-limiting step. The pseudo-second-order model provided the best fit ( $R^2 \approx 0.995$ ), indicating that chemisorption involving valence forces dominates the process. The calculated equilibrium adsorption capacity ( $q_e$ ) from the pseudo-second-order model ( $\approx 14.8$   $\text{mg/g}$ ) closely matched the experimental value (14.5  $\text{mg/g}$ ), confirming the model's validity. This behavior aligns with recent findings on green-synthesized  $\text{Fe}_3\text{O}_4$  nanoparticles for pollutant removal (Pandhare et al., 2025a; Javeria et al., 2025). The equations model:

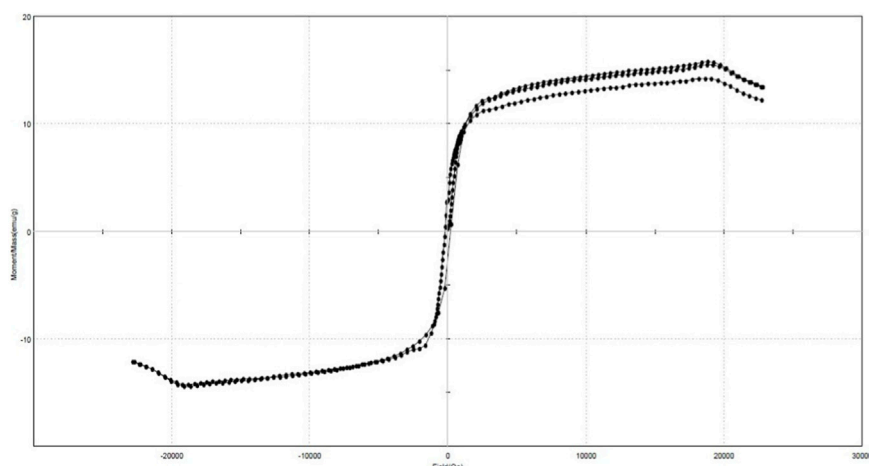


FIGURE 8 VSM analysis of Fe<sub>3</sub>O<sub>4</sub> nanoparticles.

TABLE 1 Magnetic properties of Fe<sub>3</sub>O<sub>4</sub> nanoparticles.

Saturation magnetization (emu/g)	Remnant magnetization (emu/g)	Coercivity (Oe)
15.797 emu/g	2.7242	196.89

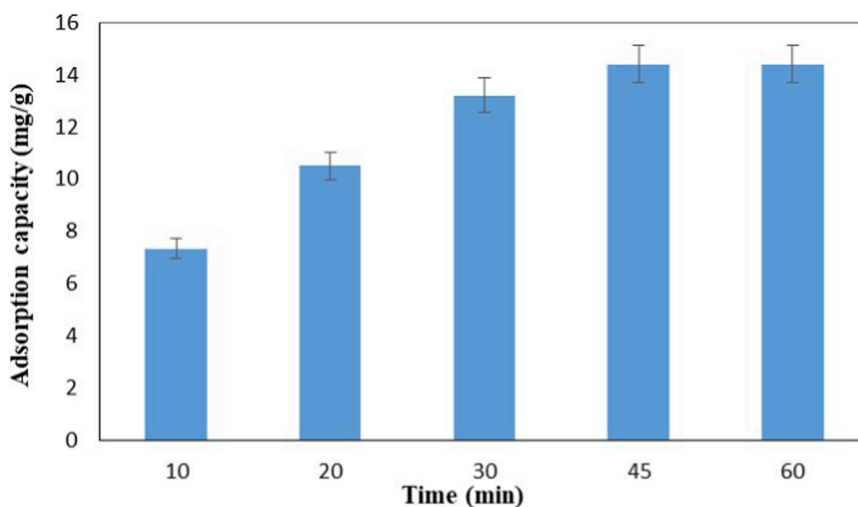


FIGURE 9 Effect of contact time on the adsorption capacity of Fe<sub>3</sub>O<sub>4</sub> nanoparticles. Experimental conditions: initial fluoride concentration (C<sub>0</sub>) = 25 mg L<sup>-1</sup>, adsorbent mass = 0.02 g, solution volume (V) = 0.03 L, pH = 7, temperature = 30 °C, and stirring speed = 200 rpm.

- Pseudo-first-order:

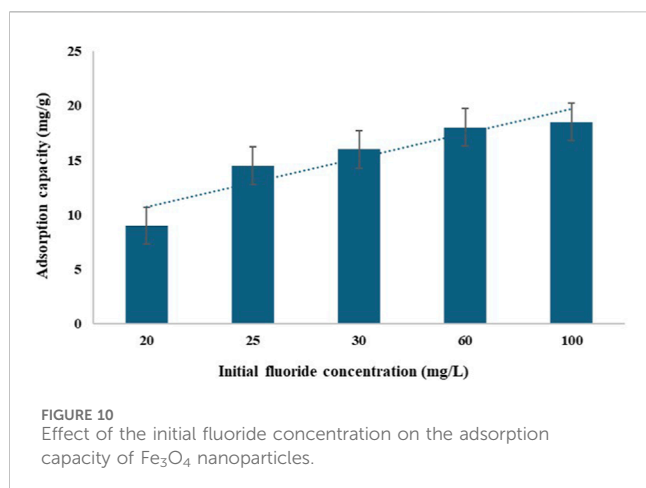
$$\log (q_e - qt) = \log q_e - \frac{k_1}{2.303} \times t$$

- Pseudo-second-order:

$$\frac{t}{qt} = \frac{1}{k_2 q_e^2} + \frac{t}{q_e}$$

### 3.2.3 Influence of the initial fluoride ion concentration

Figure 10 shows how the initial fluoride concentration affects the adsorption capacity of Fe<sub>3</sub>O<sub>4</sub> nanoparticles. The results indicate that the adsorption capacity increases as the fluoride concentration rises from 20 to 100 mg/L. This is because higher concentrations create a stronger driving force for mass transfer, allowing more fluoride ions to reach and



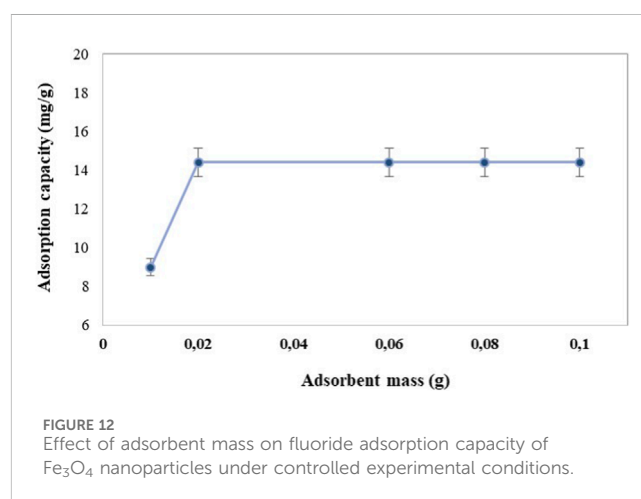
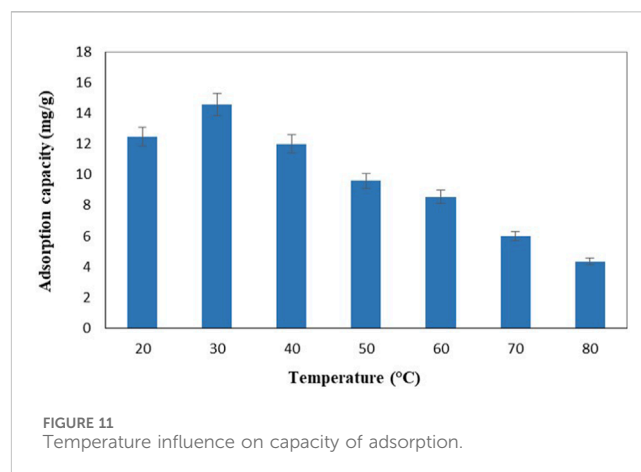
occupy the available active sites on the nanoparticle surface. As a result, a greater amount of fluoride is adsorbed per gram of nanoparticles. However, the removal efficiency (%) generally decreases at higher concentrations since the number of active sites remains constant while the amount of fluoride in solution continues to increase. This behavior is typical of adsorption systems and aligns with previous observations reported in the literature (Raul et al., 2012).

### 3.2.4 Adsorption mechanism

The fluoride adsorption onto  $\text{Fe}_3\text{O}_4$  nanoparticles synthesized via green coprecipitation is governed by multiple mechanisms. Primarily, ligand exchange occurs between surface hydroxyl groups ( $\equiv\text{Fe}-\text{OH}$ ) and fluoride ions ( $\text{F}^-$ ), forming  $\equiv\text{Fe}-\text{F}$  bonds. This process is favored under near-neutral pH conditions, where hydroxyl groups are abundant on the nanoparticle surface. Additionally, electrostatic attraction contributes due to the positive surface charge of  $\text{Fe}_3\text{O}_4$  at  $\text{pH} \approx 7$ , enhancing affinity for negatively charged fluoride ions. Surface complexation may also occur, where fluoride ions form inner-sphere complexes with Fe atoms on the nanoparticle surface. These mechanisms are consistent with recent studies on iron oxide-based adsorbents for fluoride removal (Keshta et al., 2024; Hussain et al., 2025; Armaya'u et al., 2024). The rapid initial uptake followed by equilibrium suggests chemisorption dominance, supported by strong Fe-F interactions and confirmed by kinetic modeling.

### 3.2.5 Effect of the temperature

Figure 11 shows how temperature influences fluoride adsorption by  $\text{Fe}_3\text{O}_4$  nanoparticles. The adsorption capacity increases at lower temperatures but gradually decreases as the temperature rises. This trend can be attributed to the desorption of fluoride ions from the nanoparticle surface at higher temperatures, which lowers the overall adsorption. The highest adsorption capacity, 14.5 mg/g, was recorded at 30 °C. Smitha and Thampi (2017) who found that the decrease in adsorption with increasing temperature indicates an exothermic adsorption process during fluoride removal using nanoalumina-carbon nanotubes, reported similar behavior.

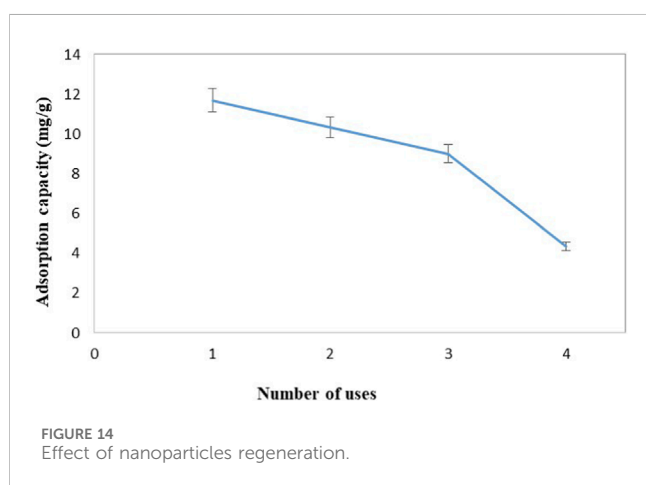
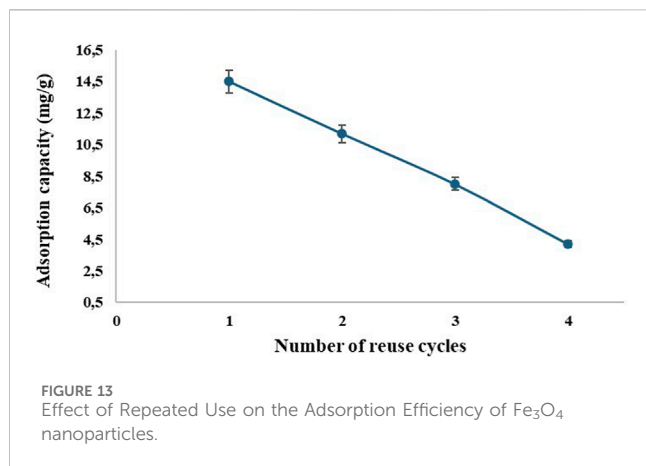


### 3.2.6 Influence of the adsorbent mass

Figure 12 shows the effect of adsorbent mass on fluoride removal using  $\text{Fe}_3\text{O}_4$  nanoparticles. Increasing the nanoparticle mass from 0.01 to 0.025 g improved fluoride removal due to the greater number of available adsorption sites. However, beyond 0.025 g, the adsorption capacity per gram of adsorbent remained nearly constant or slightly decreased. This behavior occurs because the initial fluoride concentration was kept constant, and the available fluoride ions became insufficient to fully occupy the additional surface sites of the added nanoparticles. Consequently, while the total removal efficiency increases, the adsorption capacity per gram tends to level off. The maximum adsorption capacity of approximately 14.5  $\text{mg g}^{-1}$  was obtained at 0.025 g, which represents the optimal balance between active surface area and solute availability (Qu et al., 2013).

### 3.2.7 Influence of stirring speed

Figure 13 shows how stirring speed affects the adsorption capacity of  $\text{Fe}_3\text{O}_4$  nanoparticles. The adsorption capacity increased with stirring speed, reaching a maximum of 14.5 mg/g at 200 rpm, before slightly decreasing at higher speeds. Moderate agitation improves mixing and helps fluoride ions reach the nanoparticle surface more efficiently, which enhances adsorption.



In contrast, very high stirring speeds can cause turbulence that limits contact between the adsorbent and the solution, slightly reducing efficiency. These observations are consistent with those of Chaudhary et al. (2016), who also found that an intermediate stirring rate provides the best balance between diffusion and particle stability.

### 3.2.8 Impact of nanoparticles regeneration

Restoration and recycling of nanomaterials is promising and makes nanoparticles economically viable and usable constituents. This specificity provides them an environmental advantage. A peripheral magnetic device easily and efficiently regenerated the magnetic nanoparticles. The impact of regenerating iron oxide nanoparticles was validated through multicycle adsorbents. Indeed, nanoparticles recovered after each treatment were reused to eliminate fluoride under the same optimized conditions. The adsorption efficiency decreased from one cycle to another as shown in Figure 14. This is explained by the fact that porous structures of the adsorbent enclose the remained fluoride amounts. Despite this decrease, the nanoparticles remain functional. Spent nanoparticles can occur in environmental pollution. It is therefore possible to reutilize the nanoparticles used in the treatment of contaminated water. Such conclusions are concordant with the literature; indeed, the adsorption capacity of iron oxide nano-adsorbents is well

managed succeeding recycling and several regeneration cycles (Hu et al., 2006) Nevertheless, a capacity drop subsequent to regeneration has also been detected (De Villoria et al., 2011).

### 3.2.9 Regeneration performance

The recyclability of Fe<sub>3</sub>O<sub>4</sub> nanoparticles was evaluated over five consecutive adsorption-desorption cycles. After each cycle, nanoparticles were recovered using an external magnetic field, washed with Milli-Q water, and dried at 30 °C. The adsorption efficiency decreased gradually from 44% in the first cycle to 39%, 35%, 32%, and 29% in subsequent cycles. This decline is attributed to partial pore blockage and residual fluoride ions retained within the nanoparticle structure. Despite the reduction, the nanoparticles maintained reasonable adsorption capacity, demonstrating their potential for reuse in practical applications. Similar trends have been reported for iron oxide-based adsorbents (Keshta et al., 2024; Al-Labadi et al., 2025).

### 3.2.10 Impact of nanoparticles size on the fluoride ions elimination

The curves in Figure 15 show how adsorption capacity changes over time for different nanoparticle sizes. Nanoparticles measuring 30–60 nm display slightly higher adsorption capacities than the larger ones (60–100 nm), as shown in the figure. This indicates an inverse relationship between particle size and adsorption efficiency: smaller nanoparticles can adsorb more fluoride ions. This effect is mainly due to the increase in specific surface area, meaning the surface area available per unit mass, which becomes larger as particle size decreases. The size of the nanoparticles therefore plays a crucial role in determining their adsorption performance (Kumari et al., 2019). Most of the adsorption increase is assigned to the specific surface area expansion (Yean et al., 2005). The observed results agree with those of Auffan et al. (2009). Indeed, they proved that when the size of the nanoparticles of magnetite decreases, their adsorption capacity increases thanks to the increase in the specific surface and this is due to the nanometric effect of magnetite where its surface structure generates renewed adsorption sites for polluting ions.

### 3.2.11 Effect of nanoparticles-magnetization coupling on the elimination of fluoride ions

The removal efficiency of fluoride ions improved noticeably when the Fe<sub>3</sub>O<sub>4</sub> nanoparticle treatment was combined with a magnetic field. Using nanoparticles alone resulted in a removal efficiency of 38%, while coupling them with a 1.0T magnetic field increased the efficiency to 44%. This enhancement reflects the synergistic interaction between the magnetic field and the nanoparticles, which promotes better ion mobility and stronger adsorption on the nanoparticle surface. Moreover, the eco-friendly Fe<sub>3</sub>O<sub>4</sub> nanoparticles synthesized with *Eucalyptus Globulus* extract in this study performed better than the chemically synthesized Fe<sub>3</sub>O<sub>4</sub> nanoparticles reported by Tlili et al. (2023b), which achieved about 35% fluoride removal under similar magnetic conditions. This difference suggests that the green synthesis route yields nanoparticles with more reactive surface sites and improved dispersion, leading to higher adsorption efficiency. These findings align with You et al. (2020), who emphasized that coupling magnetic devices with nano-adsorbents enhances the performance and sustainability of water purification systems. In the same context,

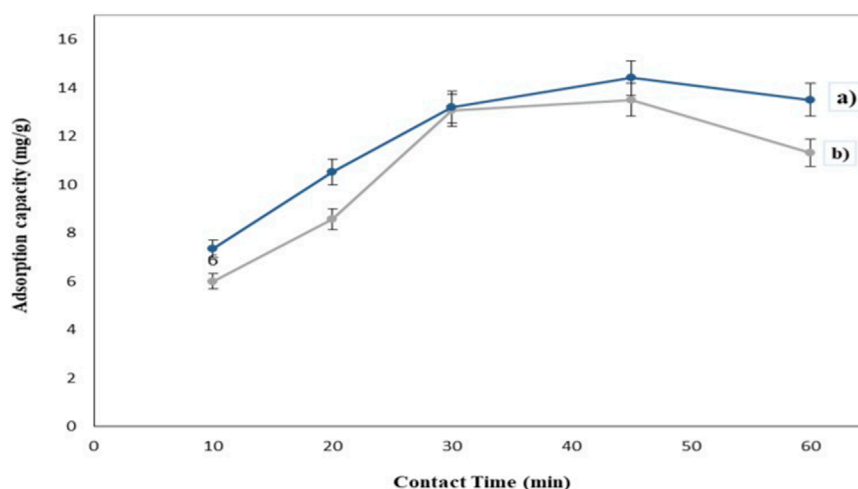


FIGURE 15 Effect of nanoparticle size (a) NPs between 30–60 nm (b) NPs between 60–100 nm.

TABLE 2 Comparison of fluoride removal efficiencies of Fe<sub>3</sub>O<sub>4</sub>-based adsorbents reported in previous studies and the present work. (Experimental conditions: pH ≈ 7, C<sub>0</sub> ≈ 25 mg/L, T ≈ 30°C).

Materials and synthesis methods	Coupling condition	Removal efficiency (E, %)	Adsorption capacity (A, mg/g)	References
Chemically synthesized Fe <sub>3</sub> O <sub>4</sub> nanoparticles	Magnetic field (1.0 T)	~35	—	Tili et al. (2023b)
Fe <sub>3</sub> O <sub>4</sub> nanoparticles (chemical coprecipitation)	Without magnetization	36	13.5	Bhatnagar et al. (2011)
Fe <sub>3</sub> O <sub>4</sub> nanoparticles (mesoporous maghemite)	Without magnetization	40	15.0	Asuha et al. (2012)
TiO <sub>2</sub> /Fe <sub>3</sub> O <sub>4</sub> green nanocomposite ( <i>Moringa oleifera</i> )	Without magnetization	41	15.8	Sbei et al. (2025)
Fe <sub>3</sub> O <sub>4</sub> nanoparticles (green synthesis using <i>Eucalyptus globulus</i> )	Magnetic field (1 T)	44	16.5	This study

Abbas et al. (2025) showed that modifying nanomaterials such as Ni-doped ZIF-67 MOF can significantly enhance adsorption performance, further supporting the importance of engineered surface properties in improving water treatment efficiency.

To better illustrate how the prepared material compares with those reported in previous studies, a concise summary is provided below. The Table 2 highlights that the green Fe<sub>3</sub>O<sub>4</sub> nanoparticles synthesized in this work under magnetic coupling conditions achieved the highest fluoride removal efficiency among the compared materials, confirming the advantage of the eco-friendly synthesis approach.

## 4 Conclusion

The green chemical production of magnetite nanoparticles was carried out by a simple and facile coprecipitation in an aqueous solution using *Eucalyptus Globulus* leaves extract as a precursor. Analysis of the SEM images showed that the Fe<sub>3</sub>O<sub>4</sub> nanoparticles had sizes ranging from 30 to 60 nm, and their ferrimagnetic nature was also confirmed. VSM analysis proved the saturation

magnetization (M<sub>s</sub>) value was measured 15.797 emu/g. The optimal adsorption factors are as follows: an initial fluoride ion concentration of 25 mg/L, a nanoparticle dose of 0.025 g/L, a temperature of 30 °C, a pH of 7, and a stirring speed of 200 rpm. Moreover, a nanoparticle-magnetization coupling clearly illustrated better treatment results for the fluoride removal with an increased adsorption capacity from 14.5 mg/g to 16.5 mg/g. Fluoride elimination increased rapidly in the beginning of the removal process to reach its maximum efficiency in 45 min with an adsorption capacity of 14.5 mg/g. The removal efficiency of fluoride ions was enhanced from 38% to 44% by coupling the use of nanoparticles and magnetic devices. In addition, the study of the regeneration of nanoparticles has shown that they remain functional but with the adsorption capacity decrease of fluoride ions.

## Data availability statement

The original contributions presented in the study are included in the article/supplementary material, further inquiries can be directed to the corresponding author.

## Author contributions

OS: Formal Analysis, Writing – original draft, Conceptualization, Methodology. AE: Validation, Funding acquisition, Writing – review and editing, Project administration, Writing – original draft, Methodology. EB: Writing – review and editing, Supervision, Validation. HT: Supervision, Formal Analysis, Writing – review and editing, Conceptualization, Visualization. AM: Formal Analysis, Writing – original draft, Conceptualization, Investigation. RS: Validation, Investigation, Writing – review and editing. MF: Writing – review and editing, Supervision, Visualization. AA: Writing – review and editing, Validation.

## Funding

The author(s) declared that financial support was received for this work and/or its publication. Federation of Arab Scientific Research Councils funded this research: Arab Research and Innovation Co-Funded Alliances grant number ARICA23\_711.

## Acknowledgements

We wish to thank the Federation of Arab Scientific Research Councils for funding and encouraging this work through Arab Research and Innovation Co-Funded Alliances (ARICA) under grant number ARICA23\_711. In addition, we thank the PRIMA-SM@WA-Medi project for its contribution in the development of

## References

- Abbas, M. Q., Javeria, H., Nazir, A., Du, Z., and Keshta, B. E. (2025). Enhanced ibuprofen removal from wastewater using Ni-doped ZIF-67 MOF: synthesis, characterization, and impact of doping on adsorption performance. *Environ. Funct. Mat.* 4, 170–182. doi:10.1016/j.efmat.2025.05.001
- Al-Labadi, I. G., Horváth, M., Alkilani, A. T., Al-Ma'abreh, A. M., Bashir, M., Keshta, B. E., et al. (2025). Simultaneous adsorptive removal of Pb<sup>2+</sup>, Cd<sup>2+</sup>, Cu<sup>2+</sup>, and Zn<sup>2+</sup> using raw Norway spruce biomass: a low-cost and eco-friendly solution for wastewater treatment. *Front. Water*. 7, 1612232. doi:10.3389/frwa.2025.1612232
- Ali, S., Thakur, S. K., Sarkar, A., and Shekhar, S. (2016). Worldwide contamination of water by fluoride. *Environ. Chem. Lett.* 14, 291–315. doi:10.1007/s10311-016-0563-5
- Amini, M., Mueller, K. I. M., Abbaspour, K. C., Rosenberg, T., Afyuni, M., Møller, K. N., et al. (2008). Statistical modeling of global geogenic fluoride contamination in groundwaters. *Environ. Sci. Technol.* 42 (10), 3662–3668. doi:10.1021/es071958y
- Armaya'u, U., Zango, M. U., Ariffin, M. M., Khalik, W. M. A. W. M., Yusoff, H. M., Zango, Z. U., et al. (2024). Copper (II) isonicotinate metal-organic framework for reusable adsorption of salmeterol from wastewater. *Sustain. Chem. One World*. 4, 100030. doi:10.1016/j.scowo.2024.100030
- Asuha, S., Zhao, Y. M., Zhao, S., and Deligeer, W. (2012). Synthesis of mesoporous maghemite with high surface area and its adsorptive properties. *Solid-State Sci.* 14 (7), 833–839. doi:10.1016/j.solidstatesciences.2012.04.011
- Auffan, M., Rose, J., Bottero, J. Y., Lowry, G. V., Jolivet, J. P., and Wiesner, M. R. (2009). Towards a definition of inorganic nanoparticles from an environmental, health and safety perspective. *Nat. Nanotechnol.* 4 (10), 634–641. doi:10.1038/nnano.2009.242
- Barbosa, L. C. A., Filomeno, C. A., and Teixeira, R. R. (2016). Chemical variability and biological activities of eucalyptus spp. essential oils. *Molecules* 21 (12), 1671. doi:10.3390/molecules21121671
- Bhatnagar, A., Kumar, E., and Sillanpää, M. (2011). Fluoride removal from water by adsorption—a review. *Chem. Eng. J.* 171 (3), 811–840. doi:10.1016/j.cej.2011.05.028
- Bustingorri, C., and Lavado, R. S. (2014). Soybean as affected by high concentrations of arsenic and fluoride in irrigation water in controlled conditions. *Agric. Water Manag.* 144, 134–139. doi:10.1016/j.agwat.2014.06.004

this research work. On the other hand, we thank the company “Delta Water” for the devices dedicated to testing.

## Conflict of interest

The author(s) declared that this work was conducted in the absence of any commercial or financial relationships that could be construed as a potential conflict of interest.

## Generative AI statement

The author(s) declared that generative AI was not used in the creation of this manuscript.

Any alternative text (alt text) provided alongside figures in this article has been generated by Frontiers with the support of artificial intelligence and reasonable efforts have been made to ensure accuracy, including review by the authors wherever possible. If you identify any issues, please contact us.

## Publisher's note

All claims expressed in this article are solely those of the authors and do not necessarily represent those of their affiliated organizations, or those of the publisher, the editors and the reviewers. Any product that may be evaluated in this article, or claim that may be made by its manufacturer, is not guaranteed or endorsed by the publisher.

- Chaudhary, M., Bhattacharya, P., and Maiti, A. (2016). Synthesis of iron oxyhydroxide nanoparticles and its application for fluoride removal from water. *J. Environ. Chem. Eng.* 4, 4897–4903. doi:10.1016/j.jece.2016.05.018

- Chiavola, A., Amato, E. D., Stoller, M., Chianese, A., and Boni, M. R. (2016). Application of iron based nanoparticles as adsorbents for arsenic removal from water. *Chem. Eng. Trans.* 47, 325–330. doi:10.3303/CET1647055

- Cronin, S. J., Manoharan, V., Hedley, M. J., and Loganathan, P. (2000). Fluoride: a review of its fate, bioavailability, and risks of fluorosis in grazed-pasture systems in New Zealand. *N. Z. J. Agric. Res.* 43 (3), 295–321. doi:10.1080/00288233.2000.9513430

- De Villoria, G. R., Hart, A. J., and Wardle, B. L. (2011). Continuous high-yield production of vertically aligned carbon nanotubes on 2D and 3D substrates. *ACS Nano* 5 (6), 4850–4857. doi:10.1021/nn2008645

- Dhakad, A. K., Pandey, V. V., Beg, S., Rawat, J. M., and Singh, A. (2018). Biological, medicinal and toxicological significance of eucalyptus leaf essential oil: a review. *J. Sci. Food Agric.* 98 (3), 833–848. doi:10.1002/jsfa.8600

- Dhillon, A., Prasad, S., and Kumar, D. (2017). Recent advances and spectroscopic perspectives in fluoride removal. *App. Spectrosc. Rev.* 52 (3), 175–230. doi:10.1080/05704928.2016.1213737

- El-Shater, R. E., Assar, S. T., Keshta, B. E., Gemeay, A. H., El-Bahnasawy, H. H., Abdel-Khalek, E. K., et al. (2024). Synthesis and study on structural, magnetic, dielectric properties and impedance spectroscopy of nanosized Mn-doped  $\gamma$ -Fe<sub>2</sub>O<sub>3</sub> for multifunctional applications. *J. Sol-Gel Sci. Technol.* 116, 1–32. doi:10.1007/s10971-024-06579-3

- Elaoud, A., Mechi, A., Tlili, H., Ferhi, M., and Hassen, H. B. (2024). Green synthesis and characterization of magnetite nanoparticles using *Eucalyptus globulus* leaves for water treatment and agronomic valorization. *Environ. Monit. Assess.* 196 (9), 786. doi:10.1007/s10661-024-12934-2

- Ganapathé, L. S., Mohamed, M. A., Mohamad Yunus, R., and Berhanuddin, D. D. (2020). Magnetite (Fe<sub>3</sub>O<sub>4</sub>) nanoparticles in biomedical application: from synthesis to surface functionalization. *Magnetochemistry* 6 (4), 68. doi:10.3390/magnetochemistry6040068

- Gemeay, A. H., Keshta, B. E., El-Sharkawy, R. G., and Zaki, A. B. (2020). Chemical insight into the adsorption of reactive wool dyes onto amine-functionalized magnetite/

- silica core-shell from industrial wastewaters. *Environ. Sci. Pollut. Res.* 27 (26), 32341–32358. doi:10.1007/s11356-019-06530-y
- Goya, G. F., Berquó, T. S., Fonseca, F. C., and Morales, M. P. (2003). Static and dynamic magnetic properties of spherical magnetite nanoparticles. *J. Appl. Phys.* 94 (5), 3520–3528. doi:10.1063/1.1599959
- Hafshejani, L. D., Tangsir, S., Daneshvar, E., Maljanen, M., Lähde, A., Jokiniemi, J., et al. (2017). Optimization of fluoride removal from aqueous solution by Al<sub>2</sub>O<sub>3</sub> nanoparticles. *J. Mol. Liq.* 238, 254–262. doi:10.1016/j.molliq.2017.04.104
- Hu, J., Chen, G., and Lo, I. M. (2006). Selective removal of heavy metals from industrial wastewater using maghemite nanoparticle: performance and mechanisms. *J. Environ. Eng.* 132 (7), 709–715. doi:10.1061/(ASCE)0733-9372(2006)132:7(709)
- Hua, M., Zhang, S., Pan, B., Zhang, W., Lv, L., and Zhang, Q. (2012). Heavy metal removal from water/wastewater by nanosized metal oxides: a review. *J. Hazard. Mat.* 211, 317–331. doi:10.1016/j.jhazmat.2011.10.016
- Hussain, M., Ali, A. S., Kousar, T., Mahmood, F., Haruna, A., Zango, Z. U., et al. (2025). Efficient removal of manganese (II) ions from aqueous solution using biosorbent derived from rice husk. *Sustain. Chem. One World.* 5, 100047. doi:10.1016/j.scowo.2025.100047
- Iiu, Y., Lv, J., Jin, W., and Zhao, Y. (2016). Defluoridation by rice spike-like akaganeite anchored graphene oxide. *RSC Adv.* 6 (14), 11240–11249. doi:10.1039/C5RA24565F
- Iseli, A., Kwen, H., and Rajagopalan, S. (2009). Nanomaterials for environmental remediation. *Nanoscale Mat. Chem.*, 649–679. doi:10.1002/9780470523674.CH20
- Ismail, R., Ibrahim, A., Mohd, H., Mahmood, M. R., and Adnan, A. (2023). Experimental data for the magnetic properties of vulcanized natural rubber nanocomposites using vibrating sample magnetometer (VSM). *Data Brief.* 46, 108872. doi:10.1016/j.dib.2022.108872
- Javeria, H., Keshta, B. E., Abbas, M. Q., Chen, S. H., Fatima, W., and Du, Z. (2025). Ultra-luminescent B, N-doped peanut shell carbon quantum dots: green synthesis for rapid on-site fluorescent detection of barium and silver ions in aqueous media. *J. Ind. Eng. Chem.* 154, 348–359. doi:10.1016/j.jiec.2025.07.001
- Jolivet, J. P., Tronc, É., and Chanéac, C. (2002). Synthesis of iron oxide-based magnetic nanomaterials and composites. *C. R. Chim.* 5 (10), 659–664. doi:10.1016/S1631-0748(02)01422-4
- Jolivet, J. P., Cassaignon, S., Chanéac, C., Chiche, D., Durupthy, O., and Portehault, D. (2010). Design of metal oxide nanoparticles: control of size, shape, crystalline structure and functionalization by aqueous chemistry. *C. R. Chim.* 13 (1-2), 40–51. doi:10.1016/j.crci.2009.09.012
- Keshta, B. E., and Gemeay, A. H. (2022). Influence of synthesis and functionalization procedures of Fe<sub>3</sub>O<sub>4</sub> NPs by Mono- and diamino silane coupling agents on the adsorption efficiency of anionic dyes. *J. Hazard. Toxic. Radioact. Waste.* 26 (1), 04021042. doi:10.1061/(asce)hz.2153-5515.0000641
- Keshta, B. E., Gemeay, A. H., Sinha, D. K., Elsharkawy, S., Hassan, F., Rai, N., et al. (2024). State of the art on the magnetic iron oxide nanoparticles: synthesis, functionalization, and applications in wastewater treatment. *Results Chem.* 7, 101388. doi:10.1016/j.rechem.2024.101388
- Kumari, P., Alam, M., and Siddiqi, W. A. (2019). Usage of nanoparticles as adsorbents for wastewater treatment: an emerging trend. *Sustain. Mat. Technol.* 22, e00128. doi:10.1016/j.susmat.2019.e00128
- Mackowiak, C. L., Grossl, P. R., and Bugbee, B. G. (2003). Biogeochemistry of fluoride in a plant–solution system. *J. Environ. Qual.* 32 (6), 2230–2237. doi:10.2134/jeq2003.2230
- Mahmed, N., Heczko, O., Söderberg, O., and Hannula, S. P. (2011). Room temperature synthesis of magnetite (Fe<sub>3</sub>O<sub>4</sub>) nanoparticles by a simple reverse coprecipitation method. *IOP conference series. Mat. Sci. Eng.* 18. doi:10.1088/1757-899X/18/3/032020
- Maiti, D., and Devi, P. S. (2015). Selective formation of iron oxide and oxyhydroxide nanoparticles at room temperature: critical role of concentration of ferric nitrate. *Mat. Chem. Phys.* 154, 144–151. doi:10.1016/j.matchemphys.2015.01.057
- Martinez, B. C., and Simeonidis, K. (2019). Magnetic nanoparticles for water purification. *Nanoscale Mat. Water Purif.* 521–552. doi:10.1016/B978-0-12-813926-4.00026-4
- Miranda, I., Lima, L., Quilhó, T., Knapic, S., and Pereira, H. (2016). The bark of *Eucalyptus sideroxylon* as a source of phenolic extracts with anti-oxidant properties. *Ind. Crops Prod.* 82, 81–87. doi:10.1016/j.indcrop.2015.12.003
- Mukhopadhyay, R., Adhikari, T., Sarkar, B., Barman, A., Paul, R., Patra, A. K., et al. (2019). Fe-exchanged nano-bentonite outperforms Fe<sub>3</sub>O<sub>4</sub> nanoparticles in removing nitrate and bicarbonate from wastewater. *J. Hazard. Mat.* 376, 141–152. doi:10.1016/j.jhazmat.2019.05.025
- O'Byrne, M., Kerzabi, B., Abbarchi, M., Lifschitz, A., Zamora, T., Malgras, V., et al. (2024). Investigation of the anatase-to-rutile transition for TiO<sub>2</sub> sol-gel coatings with refractive index up to 2.7. *Thin. Solid. Films.* 790, 140193. doi:10.1016/j.tsf.2023.140193
- Pandhare, A. B., Mulik, S. V., Patil, A. S., Sohn, D., Birajdar, N. B., Khot, V. M., et al. (2025a). Plant-mediated synthesis of biocompatible Fe<sub>3</sub>O<sub>4</sub> nanoparticles for magnetic hyperthermia therapy: a preclinical study in pharmaceutical nanotechnology. *Dev. Biol.* 530, 119–131. doi:10.1016/j.ydbio.2025.11.009
- Pandhare, A. B., Mulik, S. V., Somvanshi, S. B., Phalake, S. S., Khot, V. M., Birajdar, N. B., et al. (2025b). Polyol-crafted superparamagnetic nanoparticles: hyperthermia performance with histotoxicity assessment. *J. Indian Chem. Soc.* 102, 102195. doi:10.1016/j.jics.2025.102195
- Qu, X., Alvarez, P. J., and Li, Q. (2013). Applications of nanotechnology in water and wastewater treatment. *Water Res.* 47, 3931–3946. doi:10.1016/j.watres.2012.09.058
- Raul, P. K., Devi, R. R., Umlong, I. M., Banerjee, S., Singh, L., and Purkait, M. (2012). Removal of fluoride from water using iron oxide-hydroxide nanoparticles. *J. Nanosci. Nanotechnol.* 12 (5), 3922–3930. doi:10.1166/jnn.2012.5870
- Ravulapalli, S., and Kunta, R. (2017). Defluoridation studies using active carbon derived from the barks of *Ficus racemosa* plant. *J. Fluor. Chem.* 193, 58–66. doi:10.1016/j.jfluchem.2016.11.013
- Sbei, O., Elaoud, A., Salah, E. B., Saied, M. A. A. R. A., and Trigui, M. (2025). Effect of green TiO<sub>2</sub>/Fe<sub>3</sub>O<sub>4</sub> nanocomposites on water treatment and its agronomic application. *Surf. Interfaces* 72, 107023. doi:10.1016/j.surfin.2025.107023
- Sharma, M., Kalita, P., Senapati, K. K., and Garg, A. (2018). Study on magnetic materials for removal of water pollutants. *Emerg. Pollut.-some strategy. Qual. Preserv. Environ.*, 61–78. doi:10.5772/INTECHOPEN.75700
- Sharma, D., Bose, D., Yadav, R., Mehta, J., and Jaiswal, A. (2024). Exploring *Eucalyptus globulus* phytochemicals: analytical, antibacterial, and molecular docking investigations. *Microbe* 3, 100084. doi:10.1016/j.microb.2024.100084
- Simon-Deckers, A., Loo, S., Mayne-L'hermite, M., Herlin-Boime, N., Menguy, N., Reynaud, C., et al. (2009). Size-composition- and shape-dependent toxicological impact of metal oxide nanoparticles and carbon nanotubes toward bacteria. *Environ. Sci. Technol.* 43 (21), 8423–8429. doi:10.1021/es9016975
- Smitha, K., and Thampi, S. G. (2017). Experimental investigations on fluoride removal from water using nanoalumina-carbon nanotubes blend. *J. Water Resour. Prot.* 9 (07), 760–769. doi:10.4236/jwarp.2017.97050
- Srivastav, A. L., Singh, P. K., Srivastava, V., and Sharma, Y. C. (2013). Application of a new adsorbent for fluoride removal from aqueous solutions. *J. Hazard. Mat.* 263, 342–352. doi:10.1016/j.jhazmat.2013.04.017
- Stevens, D. P., McLaughlin, M. J., Randall, P. J., and Keerthisinghe, G. (2000). Effect of fluoride supply on fluoride concentrations in five pasture species: levels required to reach phytotoxic or potentially zootoxic concentrations in plant tissue. *Plant Soil* 227, 223–233. doi:10.1023/A:1026523031815
- Tlili, H., Elaoud, A., Asses, N., Horchani-Naifer, K., Ferhi, M., Goya, G. F., et al. (2023a). Reduction of oxidizable pollutants in waste water from the wadi El bey river basin using magnetic nanoparticles as removal agents. *Magnetochemistry* 9 (6), 157. doi:10.3390/magnetochemistry9060157
- Tlili, H., Elaoud, A., Asses, N., Horchani-Naifer, K., and Ferhi, M. (2023b). New process for the treatment of polluted water using the coupling of nanoparticles (Fe<sub>3</sub>O<sub>4</sub>) and intense magnetic system. *Emerg. Mat.* 7 (3), 947–957. doi:10.1007/s42247-023-00619-4
- Tolmacheva, V. V., Apyari, V. V., Kochuk, E. V., and Dmitrienko, S. G. (2016). Magnetic adsorbents based on iron oxide nanoparticles for the extraction and preconcentration of organic compounds. *J. Anal. Chem.* 71, 321–338. doi:10.1134/S1061934816040079
- Tran, D. L., Le, V. H., Pham, H. L., Hoang, T. M. N., Nguyen, T. Q., Luong, T. T., et al. (2010). Biomedical and environmental applications of magnetic nanoparticles. *Adv. Nat. Sci.-Nanosci. Nanotechnol.* 1 (4), 045013. doi:10.1088/2043-6262/1/4/045013
- Ugochukwu, S. C., Uche, A., and Ifeanyi, O. (2013). Preliminary phytochemical screening of different solvent extracts of stem bark and roots of *Dennettia tripetala* G. Baker. *Asian J. Plant Sci. Res.* 3 (3), 10–13. Available online at: [https://www.researchgate.net/publication/305113922\\_Preliminary\\_phytochemical\\_screening\\_of\\_different\\_solvent\\_extract\\_of\\_stems\\_bark\\_and\\_roots\\_of\\_Dennettia\\_tripetala](https://www.researchgate.net/publication/305113922_Preliminary_phytochemical_screening_of_different_solvent_extract_of_stems_bark_and_roots_of_Dennettia_tripetala).
- Yadav, N., Rani, K., Yadav, S. S., Yadav, D. K., Yadav, V. K., and Yadav, N. (2018). Soil and water pollution with fluoride, geochemistry, food safety issues and reclamation-A review. *Int. J. Curr. Microbiol. Appl. Sci.* 7, 1147–1162. doi:10.20546/ijcm.2018.705.140
- Yean, S., Cong, L., Yavuz, C. T., Mayo, J. T., Yu, W. W., Kan, A. T., et al. (2005). Effect of magnetite particle size on adsorption and desorption of arsenite and arsenate. *J. Mat. Res.* 20 (12), 3255–3264. doi:10.1557/jmr.2005.0403
- You, J., Wang, L., Zhao, Y., and Bao, W. (2020). A review of amino-functionalized magnetic nanoparticles for water treatment: features and prospects. *J. Clean. Prod.* 281, 124668. doi:10.1016/j.jclepro.2020.124668
- Zargoosh, K., Abedini, H., Abdolmaleki, A., and Molavian, M. R. (2013). Effective removal of heavy metal ions from industrial wastes using thiosalicylhydrazide-modified magnetic nanoparticles. *Ind. Eng. Chem. Res.* 52 (42), 14944–14954. doi:10.1021/ie401971w
- Zhang, W. X. (2003). Nanoscale iron particles for environmental remediation: an overview. *J. Nanopart. Res.* 5, 323–332. doi:10.1023/A:1025520116015
- Zhang, Y., Wu, B., Xu, H., Liu, H., Wang, M., He, Y., et al. (2016). Nanomaterials-enabled water and wastewater treatment. *Nano. Impact.* 3, 22–39. doi:10.1016/j.impact.2016.09.004